Isostructural Pd^{II} and Pt^{II} Pyrophosphato Complexes: Polymorphism and Unusual Bond Character in d^8−d^8 Systems
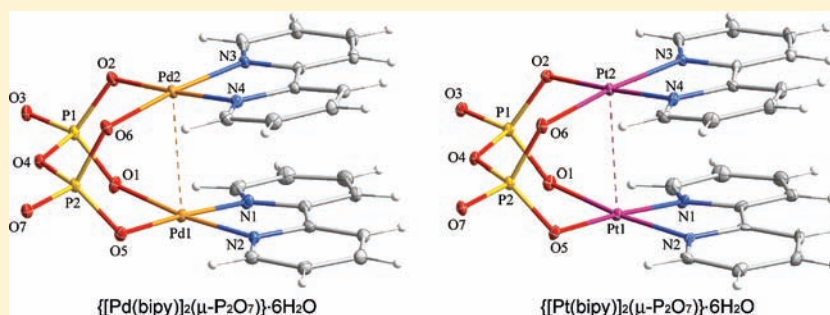
Nadia Marino,[†] Christopher H. Fazen,[†] James D. Blakemore,[‡] Christopher D. Incarvito,[‡] Nilay Hazari,*[‡] and Robert P. Doyle*[†]

[†]Department of Chemistry, Syracuse University, Syracuse, New York 13244-4100, United States
[‡]Chemistry Department, Yale University, P.O. Box 208107, New Haven, Connecticut 06520-8107, United States

S *Supporting Information*

ABSTRACT: Isostructural, "clamshell"-like, neutral dimeric pyrophosphato complexes of general formula $\{[M(bipy)]_2(\mu\text{-}P_2O_7)\}$ $[M = Pd^{II} (\mathbf{1})$ or $Pt^{II} (\mathbf{2})]$ were synthesized and studied through single-crystal X-ray diffraction, IR, ^{31}P NMR spectroscopy, and MALDI-TOF mass spectrometry. Compound **1** was synthesized through the reaction of palladium(II) acetate, 2,2′-bipyridine (bipy), and sodium pyrophosphate ($Na_4P_2O_7$) in water. Compound **2** was prepared through

{[Pd(bipy)]$_2$(μ-P$_2$O$_7$)}·6H$_2$O   {[Pt(bipy)]$_2$(μ-P$_2$O$_7$)}·6H$_2$O

two different routes. The first involved the reaction of the Pt^{IV} precursor Na_2PtCl_6, bipy, and $Na_4P_2O_7$ in water, followed by reduction in DMF. The second involved the reaction of the Pt^{II} precursor K_2PtCl_4, bipy, and $Na_4P_2O_7$ in water. Both complexes crystallize in the monoclinic chiral space group Cc as hexahydrates, $\mathbf{1}\cdot6H_2O$ (**1a**, yellow crystals) and $\mathbf{2}\cdot6H_2O$ (**2a**, orange crystals), and exhibit a zigzag chain-like supramolecular packing arrangement with short and long intra/intermolecular metal−metal distances [3.0366(3)/4.5401(3) Å in **1a**; 3.0522(3)/4.5609(3) Å in **2a**]. A second crystalline phase of the Pt species was also isolated, with formula $\mathbf{2}\cdot3.5H_2O$ (**2b**, deep green crystals), characterized by a dimer-of-dimers (*pseudo*-tetramer) structural submotif. Green crystals of **2b** could be irreversibly converted to the orange form **2a** by exposure to air or water, without retention of crystallinity, while a partial, reversible crystal-to-crystal transformation occurred when **2a** was dried in vacuo. ^{31}P NMR spectra recorded for both **1** and **2** at various pHs revealed the occurrence of a fluxional protonated/deprotonated system in solution, which was interpreted as being composed, in the protonated form, of $[HO=PO_3]^+$ (P_α) and $O=PO_3$ (P_β) pyrophosphate subunits. Compounds **1** and **2** exhibited two successive one-electron oxidations, mostly irreversible in nature; however, a dependence upon pH was observed for **1**, with oxidation only occurring in strongly basic conditions. Density functional theory and atoms in molecules analyses showed that a d^8−d^8 interaction was present in **1** and **2**.

■ INTRODUCTION

In recent years, pyrophosphate ($P_2O_7{}^{4-}$, PPi) compounds have been extensively investigated due in large part to the ubiquity of this tetra-anion in biological systems.[1−3] The multidentate nature of PPi also makes it an ideal ligand for the construction of molecule-based materials with tunable dimensionality and properties.[4] A number of PPi coordination complexes of first-row transition metal ions have now been prepared, and they have shown intriguing and varied structural motifs, biological activity, and/or magnetic properties.[4−7] On the other hand, structural reports on PPi complexes with heavy metal ions are still rare;[4] in fact, only a few Pt^{IV} monomeric compounds and a dinuclear Pt^{II} species have been structurally characterized to date.[7a]

Recently, one of us (R.P.D.) synthesized a number of Co^{II}, Ni^{II}, and Cu^{II} mono-[5a] and dinuclear[5b] pyrophosphato complexes, and these complexes demonstrated significant inhibitory concentrations against ovarian cancer cell lines.[5b] The preparation of PPi−Pt^{II}

analogues seemed a natural extension of this research, to perform comparative studies as well as mechanistic investigations. The paucity of structural reports on PPi complexes, with second- and third-row transition metal ions,[4] also inspired us to expand our studies to include Pd^{II}. In fact, we were particularly interested in the possibility of understanding the origin of the diverse chemistry exhibited by Pd^{II} and Pt^{II} d^8−d^8 dimers upon photoexcitation.[8]

Many square planar dimers of Rh^I, Ir^I, and Pt^{II} featuring a weak attractive d^8−d^8 interaction between the metal centers[9] display interesting photophysical properties and reactivity.[10] Electronic excitation results in an increase in the M−M bond order from slightly greater than zero to one (Figure 1).[8] Recently, given the scarcity of information about the chemistry, photophysical properties, and bonding of Pd^{II} analogues,[11] one of us (N.H.)
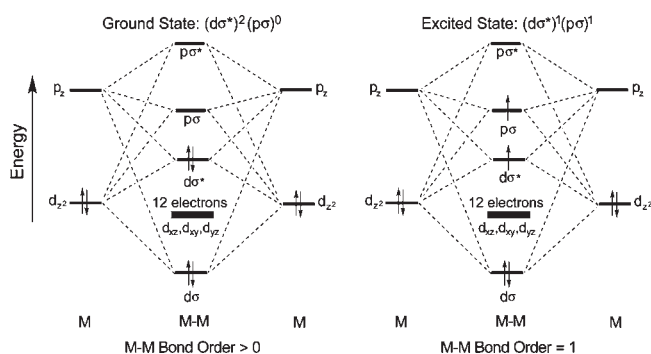
Figure 1. Orbital energy level diagrams for interactions along the metal−metal axis of two d^8 square planar units, in both ground and excited states, as applicable to Pt^{II}, Rh^I, and Ir^I dimers. Here, a weak d^8−d^8 interaction between the metal centers results from overlap in the axial direction between the valence d_{z^2} orbitals and symmetry-allowed mixing of the d_{z^2} with the $(n + 1)$ metal s and p_z orbitals. This creates four key orbitals related to metal−metal bonding in the following order of increasing energy: one strongly bonding ($d\sigma$), one weakly antibonding ($d\sigma^*$), one weakly bonding ($p\sigma$), and one strongly antibonding ($p\sigma^*$). Only the first two are filled, and hence, there is a weak metal−metal interaction. In general, the HOMO of these complexes is the weakly antibonding orbital $d\sigma^*$, and the LUMO is the weakly bonding orbital $p\sigma$.[8]

performed a study investigating the photophysical properties of a family of Pd^{II} dimers of the type $[(2\text{-phenylpyridine})Pd(\mu\text{-X})]_2$ and $[(2\text{-}p\text{-tolylpyridine})Pd(\mu\text{-X})]_2$ (X = OAc⁻, acetate; or TFAc⁻, trifluoroacetate) and examined the bonding in known Pd^{II} dimers containing short Pd−Pd distances (less than 3.10 Å).[8] We discovered that the LUMO in these systems is either a low-lying ligand-centered orbital or a $d_{x^2-y^2}$ antibonding orbital, so that the increase in Pd−Pd bond order upon HOMO−LUMO excitation only results in one-half that of the other d^8−d^8 dimers. We postulated that the reason for the noted difference in orbital ordering between the Pd^{II} and Rh^I and the Ir^I and Pt^{II} species may be related to the "intrinsic", unusually large energy gap between Pd $4d_{z^2}$ and $5s/5p$ orbitals compared with Rh^I, Ir^I, and Pt^{II}, which results in less symmetry-allowed mixing, but were unable to compare complexes with the same ligand set.[8] Thus, we set out to synthesize dimeric, isostructural Pd^{II}, and Pt^{II} pyrophosphato complexes and analyze their electronic structure.

We report here the synthesis and in-solution characterization of neutral, "clamshell"-like dimers of general formula $\{[M\text{-}(bipy)]_2(\mu\text{-}P_2O_7)\}$ [M = Pd^{II} (**1**)[12] or Pt^{II} (**2**)], where bipy =2,2′-bipyridine. In both cases, crystals were grown and analyzed through single-crystal X-ray diffraction to get one crystalline form of **1**, **1·6H₂O** (**1a**, yellow prisms) but two different phases of **2**, namely **2·6H₂O** (**2a**, orange prisms) and **2·3.5H₂O** (**2b**, deep green plates), these latter providing a rare case of polymorphism among not-monomeric Pt^{II} species. In addition, we use DFT, as well as the atom in molecules (AIM) approach to investigate the bonding in **1** and **2** and demonstrate that they have identical electronic structures.

■ EXPERIMENTAL SECTION

Materials and Methods. Solvents and chemicals were of laboratory grade and were used as received. Water was distilled and deionized to 18.6 MΩ using a Barnstead Diamond Reverse Osmosis machine coupled to a Barnstead Nano Diamond ultrapurification machine. Centrifugation was carried out on a Sorvall RT machine at 4000 rpm

for 10 min at room temperature. Infrared spectra were recorded on a Nicolet Magna-IR 850 Series II spectrophotometer as KBr pellets. FT-IR signals are reported as sh = sharp, br = broad, s = strong, m = medium, and w = weak. Electronic absorption spectra were obtained on a Varian Cary 50 Bio spectrophotometer in 1 mL quartz cuvettes between 200 and 500 nm at room temperature. For molar extinction coefficient derivations, compounds were dissolved in distilled water with final concentration in the range of 10^{-5}–10^{-6} M [**1**: max 3.3×10^{-5} M, min 4.9×10^{-6} M; **2**: max 2.4×10^{-5} M; min 4×10^{-6} M]. NMR measurements were carried out on a Bruker Avance DPX 500 MHz instrument, with samples typically made in 10% D₂O. ^{31}P NMR chemical shifts are reported with respect to 85% phosphoric acid. Aqueous 0.1% trifluoroacetic acid (TFA) and 0.1 M NaOH were used during pH-dependent experiments. Matrix-assisted laser desorption ionization time-of-flight (MALDI-TOF) mass spectrometry was performed on a Bruker Autoflex III Smartbeam machine by combining matrix and samples typically in a 5:1, 10:1, or 20:1 v/v ratio. The matrix consisted of a saturated solution of α-cyano-4-hydroxy-cinnaminic acid (CHCA) in 0.1% TFA spiked H₂O/MeCN (1:1 v/v). Elemental analysis (C, H, N) were performed by QTI Intertek, Whitehouse, NJ.

Synthesis of $[Pd(bipy)]_2(\mu\text{-}P_2O_7)$ (1). Palladium(II) acetate (0.2245 g, 1 mmol), 2,2′-bipyridine, bipy, (0.1249 g, 0.8 mmol), and sodium pyrophosphate tetrabasic, Na₄P₂O₇, (0.1595 g, 0.6 mmol) were dissolved in 50 mL of water at 60 °C with stirring, and the reaction mixture was left for 2 h. Suitable crystals for X-ray diffraction, identified then as **1·6H₂O** (**1a**), were obtained within a few days by slow evaporation of the solvent at room temperature. Yield 85% based on bipy (limiting reagent). Analytical data for **1·5.5H₂O** (after drying overnight in vacuo), $C_{20}H_{27}N_4O_{12.5}P_2Pd_2$ (MW = 798.24 g/mol): Calcd. C, 30.09; H, 3.41; N, 7.02. Found: C 30.12, H 3.58, N 7.05. FTIR (KBr): 3403(br), 3077(sh), 1638(br), 1449(sh), 1203(s), 1112-(sh), 1035(s), 1001(sh), 876(w), 767(sh) cm⁻¹. MS (MALDI-TOF): $[M + H]^+$ requires m/z 700; found 699.72. ^{31}P NMR (10% D₂O) (δ): 10.74 ppm (pH 4−5); 2.82 ppm (pH 10). UV−vis (H₂O): λ_{max}/nm (ε/ $M^{-1}cm^{-1}$) 208.0 (87200); 241.0 (41900); 304.0 (32800).

Synthesis of $[Pt(bipy)]_2(\mu\text{-}P_2O_7)$ (2). *Method A.* Sodium hexachloroplatinate(IV), Na₂PtCl₆, (0.5619 g, 1 mmol), bipy, (0.1249 g, 0.8 mmol), and Na₄P₂O₇, (0.2659 g, 1 mmol) were dissolved in 50 mL of water at 60 °C with stirring, resulting in a bright yellow solution. The reaction mixture was left to react for 2 h at this temperature. Yellow needle-shaped crystals precipitated as the solution cooled, and these were separated by centrifugation and identified as $Pt(bipy)Cl_4$[13] via single-crystal X-ray diffraction (Supporting Information). DMF was then added to the filtered solution in a 1:1 v/v ratio, and several crystallization vials were prepared by layering 5 mL of this new solution with 5 mL of CH₂Cl₂. Dark orange prismatic crystals of **2·6H₂O** (**2a**), suitable for X-ray analysis, were observed within several months (estimated yield 20−25%), together with traces of well-shaped, deep green plates of **2·3.5H₂O** (**2b**).

Method B. Potassium tetrachloroplatinate(II), K₂PtCl₄, (0.4151 g, 1 mmol), bipy (0.1249 g, 0.8 mmol), and Na₄P₂O₇ (0.2659 g, 1 mmol) were dissolved in 50 mL of water at 60 °C with stirring, and the reaction mixture was left to react for about 45 min at this temperature. A brown powder precipitated out of the pale yellow-brown solution, and this was collected by centrifugation and subsequently dissolved in hot DMSO, resulting in a dark-yellow-brown solution. X-ray quality crystals of **2·3.5H₂O** (**2b**) grew as deep green plates from the DMSO solution after about one month (estimated yield 5−10%). When filtered from the DMSO solution and exposed to humidity in the air, those crystals rapidly converted to the orange form (vide infra). Preliminary attempts to produce a Pt^{III} dimer via oxidation with HNO₃/NaNO₂ failed, resulting instead in the isolation of the Pt^{IV} monomer of formula $Pt(bipy)$-$(NO_2)_2Cl_2$ (**3**, Supporting Information). Analytical data for **2·4.5H₂O** (after drying **2a** overnight in vacuo), $C_{20}H_{25}N_4O_{11.5}P_2Pt_2$

Table 1. Summary of Crystal Data for $\{[Pd(bipy)]_2(\mu\text{-}P_2O_7)\}\cdot 6H_2O$ (1a), $\{[Pt(bipy)]_2(\mu\text{-}P_2O_7)\}\cdot 6H_2O$ (2a), $\{[Pt(bipy)]_2(\mu\text{-}P_2O_7)\}\cdot 3.5H_2O$ (2b), and $\{[Pt(bipy)Cl_2(NO_2)_2]\}$ (3)

compound	$1\cdot 6H_2O$ (1a)	$2\cdot 6H_2O$ (2a)	$2\cdot 3.5H_2O$ (2b)	3
formula	$C_{20}H_{28}N_4O_{13}P_2Pd_2$	$C_{20}H_{28}N_4O_{13}P_2Pt_2$	$C_{20}H_{23}N_4O_{10.5}P_2Pt_2$	$C_{10}H_8Cl_2N_4O_4Pt$
M_r	807.20	984.58	939.54	514.19
crystal system	monoclinic	monoclinic	monoclinic	triclinic
space group	Cc	Cc	$C2_1/c$	$P\text{-}1$
a (Å)	16.5454(8)	16.5752(8)	22.472(4)	8.809(2)
b/Å	12.5799(8)	12.5881(8)	12.765(2)	9.011(2)
c (Å)	13.4291(8)	13.5528(8)	18.517(3)	10.564(2)
α (deg)	90	90	90	98.40(2)
β (deg)	105.905(1)	105.973(1)	111.797(8)	104.943(4)
γ (deg)	90	90	90	118.56(1)
V (Å^3)	2688.1(3)	2718.6(3)	4932(1)	674.8(2)
Z	4	4	8	2
D_c (g cm^{-3})	1.995	2.406	2.531	2.531
T (K)	98(2)	223(2)	98(2)	223(2)
$F(000)$	1608	1864	3528	480
μ (Mo K_α) (mm^{-1})	1.531	10.471	11.485	10.813
refl. collected	6192	5997	25756	7050
refl. indep. (R_{int})	6192 (0.0000)	5997 (0.0000)	5907 (0.0829)	3072 (0.0361)
refl. obs. $[I > 2\sigma(I)]$	6040	5744	4564	2681
$R_1{}^a$ $[I > 2\sigma(I)]$ (all)	0.0207 (0.0216)	0.0209 (0.0224)	0.0513 (0.0734)	0.0338 (0.0457)
$wR_2{}^b$ $[I > 2\sigma(I)]$ (all)	0.0484 (0.0490)	0.0413 (0.0418)	0.0865 (0.0923)	0.0604 (0.0638)
goodness-of-fit on F^2	1.041	0.827	1.169	1.064
abs. struct. param.	0.000(14)	0.003(5)	—	—
$\Delta\rho_{max,\,min}$ (eÅ^{-3})	0.637 and -0.394	1.256 and -0.984	1.300 and -1.432	1.164 and -1.000

^{a} $R_1 = \sum(|F_o| - |F_c|)/\sum|F_o|$. ^{b} $wR_2 = \{\sum[w(F_o{}^2 - F_c{}^2)^2]/\sum[w(F_o{}^2)^2]\}^{1/2}$ and $w = 1/[\sigma^2(F_o{}^2) + (mP)^2 + nP]$ with $P = (F_o{}^2 + 2F_c{}^2)/3$, $m = 0.0270$ (1a), 0.0000 (2a), 0.0254 (2b), 0.0233 (3), and $n = 0.0000$ (1a), 0.0000 (2a), 34.0724 (2b), 0.9889 (3).

(MW = 957.54 g/mol): Calcd. C, 25.09; H, 2.63; N, 5.85. Found: C 24.55; H, 2.18; N, 5.86. FTIR (KBr): 3448(br), 3077(sh), 1634(s), 1454(s), 1214(s), 1192(s), 1036(sh), 1001(sh), 878(w), 776(sh) cm^{-1}. MS (MALDI-TOF): $[M + H]^+$ requires m/z 877; found 877.02. ^{31}P NMR (10% D_2O) (δ): 14.03 ppm (pH 3.5−6.8); 2.85 ppm (pH 11). UV−vis (H_2O): λ_{max}/nm (ε/M^{-1}cm^{-1}) 203.0 (42700); 248.0 (38500); 307.0 (21000); 320.0 (16800); 363.0 (3850).

Crystal Structure Determination and Refinement. X-ray crystallographic data for 1a and 2a were collected with a Bruker-AXS SMART CCD diffractometer at 98 K using graphite monochromated Mo K_α radiation ($\lambda = 0.71073$ Å). The crystals where coated with Paratone oil, attached to a glass fiber, and quickly transferred under the cold nitrogen stream of the diffractometer. For data collection and integration, the Bruker SMART[14] and SAINT[15] softwares were employed. Empirical absorption corrections were calculated using SADABS.[16] The structures were solved by direct methods and subsequently completed by Fourier recycling using the SHELXTL[17] software packages and refined by the full-matrix least-squares refinements based on F^2 with all observed reflections (Friedel opposites not merged). All non-hydrogen atoms were refined anisotropically. The hydrogen atoms on water molecules of crystallization in the structures of 1a and 2a were located on the ΔF map and refined with restraints, with thermal factors fixed to 0.04 Å^2; hydrogen atoms on the bipy ligands were refined using a riding model.

X-ray crystallographic data for 2b and 3 were collected with a Rigaku Mercury 275R CCD (SCX mini) diffractometer at 223 K using graphite monochromated Mo,K_α radiation. Data were collected and processed using CrystalClear (Rigaku).[18] Data were corrected for Lorentz and polarization effects; an empirical absorption correction was applied as well. The structures were solved by direct methods,[19] expanded using Fourier techniques and refined by the full-matrix least-squares refinements based on F^2 with all observed reflections. The non-hydrogen atoms were refined anisotropically, except O(1w) in the structure of 2b, to which only half occupation has been assigned because of disorder. This water molecule, in fact, occupies a position close to a symmetry element (the screw axis), which generates a symmetry-related water position at a distance of only 1.18 Å. Hydrogen atoms on water molecules of crystallization in 2b were neither found nor calculated; hydrogen atoms on the bipy ligands were refined using a riding model. Neutral atom scattering factors were taken from Cromer and Waber.[20] Anomalous dispersion effects were included in F_{calcd};[21] the values for $\Delta f'$ and $\Delta f''$ were those of Creagh and McAuley.[22] The values for the mass attenuation coefficients are those of Creagh and Hubbell.[23] All calculations were performed using the CrystalStructure[24] crystallographic software package except for refinement, which was performed using SHELXL-97.[17] Crystal data for 1a−3 are summarized in Table 1. Selected bond lengths and angles for each compound are collected in Table 2, while information related to hydrogen bonds is given in the Supporting Information. CCDC reference numbers are 801206−801209.

Electrochemistry. Electrochemical measurements were made on a Princeton Applied Research Versastat 4−400 potentiostat/galvanostat using a standard three-electrode configuration. A basal plane graphite electrode (surface area: 0.09 cm^2) was used as the working electrode to minimize background water oxidation. The electrode consisted of a brass cylinder, sheathed in a Teflon tube. At the tip of the brass, a two-part Ag conducting epoxy (Alfa Aesar) was used to firmly attach the basal plane carbon electrode surface to the brass. Finally, the tip was sealed with the organic solvent-resistant, electrically insulating, two-part epoxy Tra-bond 2151 (Emerson and Cuming, Canton, MA). Immediately prior to experiments, the working electrode was polished with 1 μm

Table 2. Selected Bond Distances (Å) and Angles (deg) for 1a, 2a, and 2b[a]

	1a	2a	2b
M1−O1	2.027(2)	2.036(4)	2.019(5)
M1−O5	2.019(2)	2.038(3)	2.018(6)
M1−N1	1.992(2)	1.991(4)	1.953(7)
M1−N2	1.985(3)	1.975(4)	1.970(7)
M2−O2	2.030(2)	2.049(4)	2.018(6)
M2−O6	2.015(2)	2.031(3)	2.016(6)
M2−N3	1.990(2)	1.987(4)	1.968(8)
M2−N4	1.988(2)	1.974(4)	1.971(7)
M1···M2	3.0366(3)	3.0522(3)	3.0318(6)
O1−M1−O5	91.73(8)	90.4(1)	89.5(2)
O1−M1−N1	92.8(1)	93.8(2)	93.8(3)
O1−M1−N2	172.6(1)	173.6(2)	173.7(3)
O5−M1−N1	175.3(1)	175.4(2)	176.3(3)
O5−M1−N2	94.2(1)	94.8(2)	94.9(3)
N1−M1−N2	81.3(1)	81.1(2)	81.7(3)
O2−M2−O6	91.1(1)	89.6(1)	92.0(2)
O2−M2−N3	94.0(1)	95.2(2)	92.7(3)
O2−M2−N4	175.6(1)	176.6(2)	174.5(3)
O6−M2−N3	173.9(1)	174.0(2)	175.2(3)
O6−M2−N4	93.4(1)	93.8(2)	93.3(3)
N3−M2−N4	81.5(1)	81.5(2)	82.0(3)

[a] Symmetry operation used to generate equivalent atoms for **1a**, **2a**: (a) $x, 1 - y, -0.5 + z$; for **2b**: (a) $1.5 - x, 0.5 - y, 1 - z$; (b) $+x, 1 + y, +z$. See Figure 6.

alumina paste, washed with copious amounts of water, and allowed to dry completely. Then, the surface of the working electrode was resurfaced with tape to restore the gray, basal surface. For aqueous electrochemical experiments, a platinum wire was used as the counter electrode, and a Ag/AgCl reference electrode (Bioanalytical Systems, Inc.) was used as the reference electrode (NHE vs Ag/AgCl: $+197$ mV). Experiments were carried out in unbuffered solutions containing 0.1 M KNO$_3$ (Johnson Matthey, electronics grade) as the supporting electrolyte.

Computational Details. All geometry optimizations were performed using Gaussian 09 Revision A.02.[25] The LANL2DZ basis set was used for Pd and Pt, and the 6-31G++(d,p) basis set was used for all other atoms. The LANL2DZ pseudopotential was used for Pd and Pt. Frequency calculations were performed on all optimized structures to ensure that they were true minima. Fragment analysis was performed using the Amsterdam Density Functional (Version ADF2007.01) package, with the geometry determined from the Gaussian optimization.[26] TZP basis sets were used with triple-ξ accuracy sets of Slater-type orbitals, with polarization functions added to all atoms. Relativistic corrections were made using the ZORA (zero-order relativistic approximation) formalism,[27] and the core electrons were frozen up to 1s for C, N, O, and F, 2p for P and Cl, 3d for Pd, and 4d for Pt. The local density approximation of Vosko, Wilk, and Nusair[28] was utilized. All quoted electronic structure data from optimized structures use an integration grid of 6.0. The fragment analyses used the MOs of the chosen fragments as the basis set for the molecular calculation, and initial spin restricted calculations were carried out on the fragments with the geometry that they had in the molecule; thus, the fragments were in a prepared singlet state. Neutral fragments were chosen as this assisted in drawing up the MO diagrams. Topological analyses of the electron density were performed using the XAIM program,[29] which located and characterized the critical points.
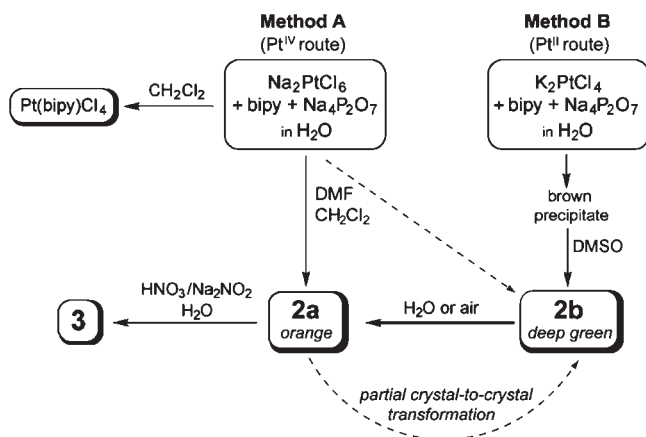
■ RESULTS AND DISCUSSION

Synthesis and Characterization. Compound **1** was synthesized in good yield by reacting palladium(II) acetate, either in its monomeric Pd(OAc)$_2$ or trimeric $[Pd(OAc)_2)]_3$ form, with solid bipy and sodium pyrophosphate in water, in a *quasi*-stoichiometric molar ratio. The reaction mixture was stirred and heated at 60 °C for two hours. Typically, bipy was added to the Pd^{II} salt solution in less than the required 1:1 molar ratio to minimize any loss of metal as a homoleptic bipy species (as found in the ESI mass spectrum of the crude stoichiometric reaction), while PPi was added in slight excess (0.6:1 vs 0.5:1 molar ratio) to ensure metal coordination. Prismatic yellow crystals with composition **1**·6H$_2$O (**1a**) were grown by slow evaporation of the mother liquor in about a week. Palladium(II) chloride, dissolved in water by means of KCl addition, was also used as a source of Pd^{II}. In this case, a larger excess of PPi (typically 4−5 fold) was required to form the dimer, presumably due to the considerable amount of chloride ions in solution competing for metal coordination. A third route via Pd(bipy)(NO$_3$)$_2$ as starting material has also been reported by ref 12.

Compound **1a** was characterized by elemental analysis, powder and single-crystal X-ray diffraction, ^{31}P NMR and IR spectroscopy, and mass spectrometry. The IR spectrum of **1a** as a KBr pellet showed a large broad band centered at 3403 cm^{-1} and a small sharper one at 3077 cm^{-1} due to the presence of water molecules involved in hydrogen bonding; bands associated to the bipy ligand are observed at 1693 and 1449 cm^{-1}.[30] The pyrophosphate P−O stretch, which usually appears as a broad band centered around 1100 cm^{-1} with shoulders at $\pm 30-100$ cm^{-1}, appeared instead as two sharp bands at 1036 and 1001 cm^{-1}, suggesting a strong dependence on the coordination environment, as already pointed out elsewhere.[5i] MALDI-TOF mass spectrometry performed using water or aqueous 0.1 M KNO$_3$ solutions of **1a** gave the $[M + H]^+$ ion centered at m/z 700 $[\{H[Pd(bipy)]_2(P_2O_7)\}^+]$. Other relevant fragments, such as $\{[Pd(bipy)]_2(PO_4)\}^+$ (m/z 620) and $\{H[Pd_2bipy](P_2O_7)\}^+$ (m/z 545), were also identified. In each case, the observed patterns were consistent with the natural isotopic distribution (Supporting Information).

Compound **2** was prepared using two different routes, summarized in Scheme I. In the first route (method A), a solution containing sodium hexachloroplatinate(IV), bipy, and sodium pyrophosphate in a 1:0.8:1 ratio was reacted in pure water for 2 h at 60 °C. The solution was cooled to room temperature, and then DMF was added to prepare a 1:1 v/v solution. Layering with dichloromethane generated orange crystals after seven to eight months, which were confirmed as $\{[Pt(bipy)]_2(\mu\text{-}P_2O_7)]\cdot 6H_2O\}$ (**2a**) by X-ray crystallography. This synthetic method was highly reproducible, although the yield of **2** was only around 20−25% after crystallization. We believe that DMF is the reductant for the reduction of Pt^{IV} to Pt^{II}.[31] If the reaction was performed in absence of DMF, we obtained high-quality single crystals of Pt(bipy)Cl$_4$,[13] with no evidence for a Pt^{II} product (Supporting Information). Along with the isolated orange crystals of **2a**, small dark green plates were also observed in the reaction mixture. They usually appeared, in trace quantities, after the removal of the first aliquot of orange crystals from the reaction mixture. Single-crystal X-ray diffraction experiments determined that these crystals were a different polymorph of **2**, with composition **2**·3.5H$_2$O (**2b**).

Investigation of the H$_2$O/DMF reaction mixture via MALDI-TOF spectrometry indicated that the formation of **2** is a very slow

Scheme I. Compound 2

Figure 2. (Left) Rapid transformation of **2b** (deep green) into **2a** (orange) with the crystals being in touch with a minimum amount of water. (Right, a–d) Monitoring the drying effect on X-ray quality crystals of **2a** (orange): Note the transition from a bright orange color to opaque "black". (e) Effect of adding a drop of water into the vial containing the dried crystals (d).

process, given that the complex could only be detected in solution after several weeks. Dimer formation could be accelerated by adding a larger excess of pyrophosphate and heating for longer times. In particular, an aqueous solution containing Na_2PtCl_6, bipy, and $Na_4P_2O_7$ in a 1:1:2 molar ratio was prepared and incubated at 50 °C for two weeks. This solution was mixed with DMF in a 1:1 v/v ratio and then separated in several vials and layered with CH_2Cl_2. X-ray quality crystals of **2a** (but not **2b**) were observed growing at the interface after 4–5 weeks in low yield.

Compound **2** was also synthesized starting directly from Pt^{II} (method B). In this case, potassium tetrachloroplatinate(II), bipy, and sodium pyrophosphate were mixed in water in a 1:0.8:1 ratio. The reaction was heated at 60 °C for 30–45 min, resulting in a pale yellow-brown solution (longer reaction times resulted in the precipitation of a certain amount of black Pt^0). The reaction mixture was allowed to cool to room temperature, which caused a brown powder to precipitate out of solution. After centrifugation, the solution was decanted, and the precipitate was dissolved in hot DMSO, producing a dark yellow-brown solution. X-ray quality crystals of **2b** appeared in this solution after about one month, as deep green ("black") plates. Although this method could be repeated with a high level of reproducibility, analysis of the dried brown precipitate from the initial reaction mixture using IR spectroscopy did not suggest the presence of any pyrophosphate in the sample. Moreover, if this dried precipitate was dissolved in hot DMSO, no crystal formation was observed. On the basis of the IR spectrum and the solubility in hot DMSO, we hypothesize that this initial precipitate may be $Pt(bipy)Cl_2$.[32] Compound **2** only crystallizes because of the small amount of pyrophosphate incorporated in the reaction mixture as a consequence of the decanting process. This appears to be consistent with the extremely low yield detectable via this route (estimated 5–10% based on Pt). However, we have been unable so far to generate **2** in control experiments involving preformed Pt-(bipy)Cl_2 dissolved in DMSO in the presence of sodium pyrophosphate. This suggests that the exact concentration of the reagents may play an important role, and that the system requires further investigation to be fully understood.

Interestingly, the deep green crystals of **2b** obtained as a major product from method B and a minor product from method A turned orange very rapidly when left standing in air on filter paper or exposed to a minimum amount of water (Figure 2). We believe that this color change is caused by incorporation of
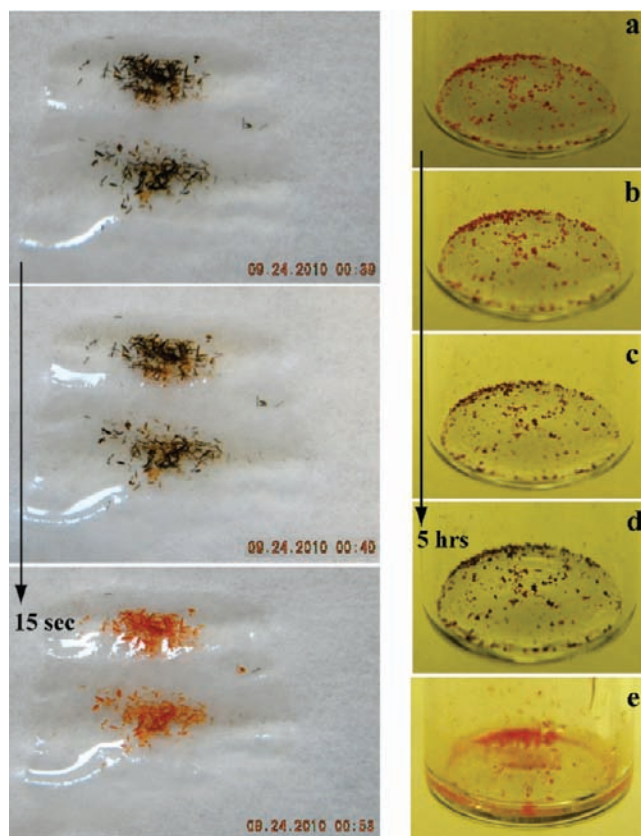
additional solvent molecules in the crystal, resulting in larger dimer–dimer separation. X-ray diffraction analysis (vide infra) strongly supports this hypothesis, as the orange polymorph contains more water molecules than the deep green one. The process did not happen with retention of crystallinity, and orange crystals obtained by solvation of the deep green crystals were not suitable for X-ray diffraction. Further support for the proposal that the color change is attributable to different levels of solvation was obtained from the following experiment: when X-ray quality crystals of **2a** grown following method A were dried in vacuo, a progressive and slow color change from bright orange to opaque "black" was observed, presumably as some solvent was removed. Complete conversion to a black material did not happen even after prolonged drying in vacuo, and the material returned back to the "original" bright orange color after a few minutes of exposure to air. This "reconversion" to the orange product occurs instantaneously with addition of a drop of water to the partially opaque-"black" crystals (Figure 2 and Figures S1–S2 of the Supporting Information).

Elemental analysis conducted on a crystalline sample of **2a** dried overnight in vacuo were consistent with the formulation $2 \cdot 4.5H_2O$. This supports our hypothesis that **2a** cannot be fully converted to **2b**. The infrared spectra of **2a** and **2b** as KBr pellets in the range 4000–400 cm^{-1} were superimposable and almost identical to the spectrum of **1a**, showing again the pyrophosphate P–O stretch as two sharp bands at 1036 and 1001 cm^{-1}.
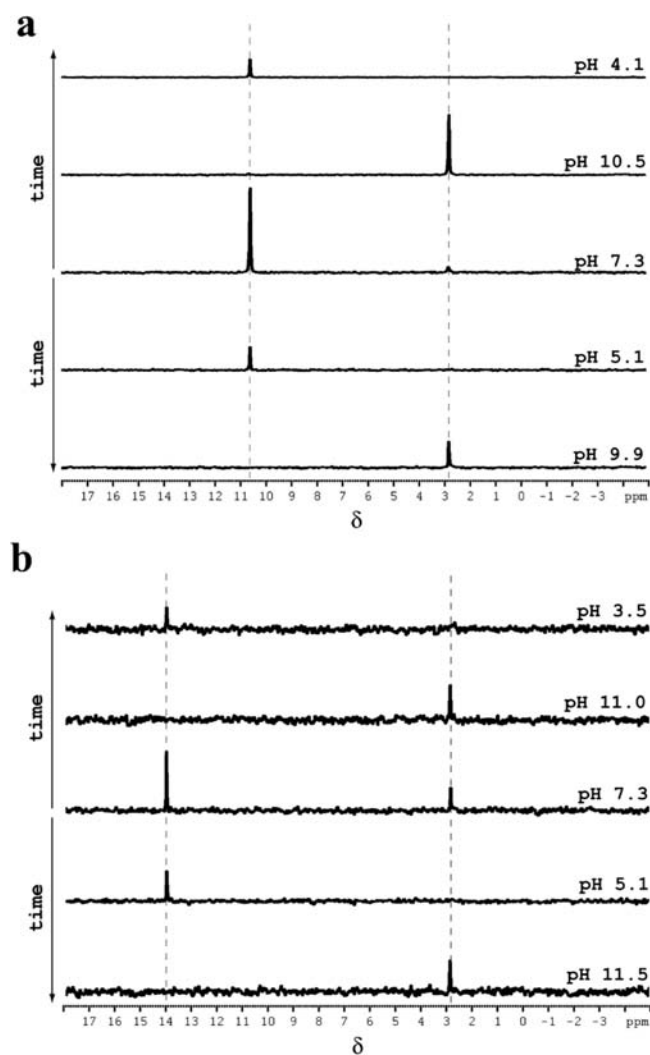
Figure 3. ^{31}P NMR spectra of **1** (a) and **2** (b) in H_2O (10% D_2O) recorded at various pHs. For analogous plots in aqueous 0.1 M KNO_3 (Supporting Information).

MALDI-TOF mass spectrometry performed using water or aqueous 0.1 M KNO_3 solutions of **2a**/**2b** gave the $[M + H]^+$ ion centered at m/z 877 $[\{H[Pt(bipy)]_2(P_2O_7)\}^+]$, as well as the sodium and potassium adducts $[M + Na]^+$ (m/z 899) and $[M + K]^+$ (m/z 915), respectively. The fragment $\{[Pt(bipy)]_2(PO_4)\}^+$ (m/z 797) was also identified. In each case, the observed patterns were consistent with the natural isotopic distribution (Supporting Information). ^{31}P NMR and electronic absorption spectra (vide infra) of either **2a** or **2b** dissolved in water were identical.

^{31}P NMR Characterization. ^{31}P NMR spectra of **1a** and either **2a** or **2b** recorded at various pHs [approximate range 3.5−12] in pure water or aqueous 0.1 M KNO_3 solutions unexpectedly displayed two different peaks at pHs close to neutrality (Figure 3 and Figure S3 of the Supporting Information), indicating the presence of (i) two different species or (ii) two nonequivalent phosphate atoms, P_α (A) and P_β (B). As the pH was lowered or raised, full conversion to a single product was observed, suggesting the occurrence of an equilibrium between protonated−deprotonated states of the PPi anion [hypothesis (i)]. The exact site of protonation is unknown but presumably occurs at one of the P=O bonds (Scheme II). The

Scheme II. AA Ab, and BB Systems
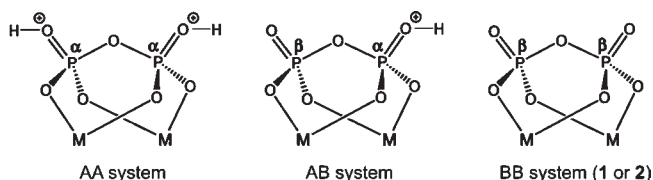
Possible protonation/deprotonation pathways:

(a) AA ⟷ AA+BB ⟷ BB

(b) AB ⟷ AB+BB ⟷ BB

protonation event is fully reversible, and it is possible to cycle between **1** or **2** and the protonated species, with no decomposition. Clearly, the product of protonation is either symmetrical or fluxional on the NMR time scale, as only one phosphorus environment is observed at low pH. Two possible explanations can be found to justify the observed situation: (a) the existence of a symmetrical AA + BB system ($H_2P_2O_7^{2-}$ + $P_2O_7^{4-}$: $2P_\alpha$ + $2P_\beta$) at neutral pH, with form BB being prevalent at high pH values and form AA prevalent at low pH values or (b) the occurrence of an "AB (low pH) − (AB + BB) (neutral pH) − BB (high pH)" type of pH-dependent equilibrium, where the intermediate AB is only protonated at one phosphorus atom. In this case, fast proton exchange on the NMR time scale presumably results in only one ^{31}P resonance for AB. In both cases, the singlet observed at high pH should be attributed to **1** or **2** (with two equivalent P_β atoms). Mass spectrometry data revealed the presence of the $[M + H]^+$ ion in acidic solutions of **1** and **2**. On this basis, we believe that route (b) is most likely to describe the in-solution behavior of these systems, especially given that a double protonation of the PPi would greatly increase the possibility that the ligand would dissociate completely. It should be noted that a third hypothesis could have been made, i.e., the existence of a nonfluxional AB system ($HP_2O_7^{3-}$: P_α + P_β) at neutral pH, which gradually interconverts into symmetrical AA ($H_2P_2O_7^{2-}$: $2P_\alpha$) or BB ($P_2O_7^{4-}$: $2P_\beta$) when approaching acidic or basic pHs, respectively. This, however, would have required the observation of identical integrations for the two peaks observed around neutral pH, which we do not observe.

Chemical shift data (water solution) for the protonated−deprotonated species are 10.74 (P_α) and 2.82 (P_β) ppm for **1** and 14.03 (P_α) and 2.85 (P_β) ppm for **2**, respectively. Only minimal differences can be observed between the spectra recorded in water or 0.1 M KNO_3 solutions, with both peaks shifted by about +0.1 ppm in the latter case with respect to the former. These numbers are in good agreement with chemical shift values in the range of 1.8−2.4 reported by Bose et al. for fully deprotonated monomeric Pt^{II} and Pt^{IV} pyrophosphato complexes.[7a]

Solid State Structures of $\{[Pd(bipy)]_2(\mu-P_2O_7)\}\cdot6H_2O$ ($1\cdot6H_2O = 1a$), $\{[Pt(bipy)]_2(\mu-P_2O_7)\}\cdot6H_2O$ ($2\cdot6H_2O = 2a$), **and** $\{[Pt(bipy)]_2(\mu-P_2O_7)\}\cdot3.5H_2O$ ($2\cdot3.5H_2O = 2b$). The solid state structures of compounds **1** and **2** consist of neutral, "clamshell"-like dimers made up of two [metal-(bipy)]$^{2+}$ units linked together by a classical bis-bidentate tetra-anionic pyrophosphate group. The geometry around the metal center is distorted square planar. Compound **1** crystallizes in the monoclinic chiral Cc space group as hexahydrate, $1\cdot6H_2O$ (**1a**, see also ref 12), while **2** exists in two solid-state forms: $2\cdot6H_2O$ (**2a**) (Cc space group, orange polymorph) and $2\cdot3.5H_2O$ (**2b**) ($C2_1/c$ space
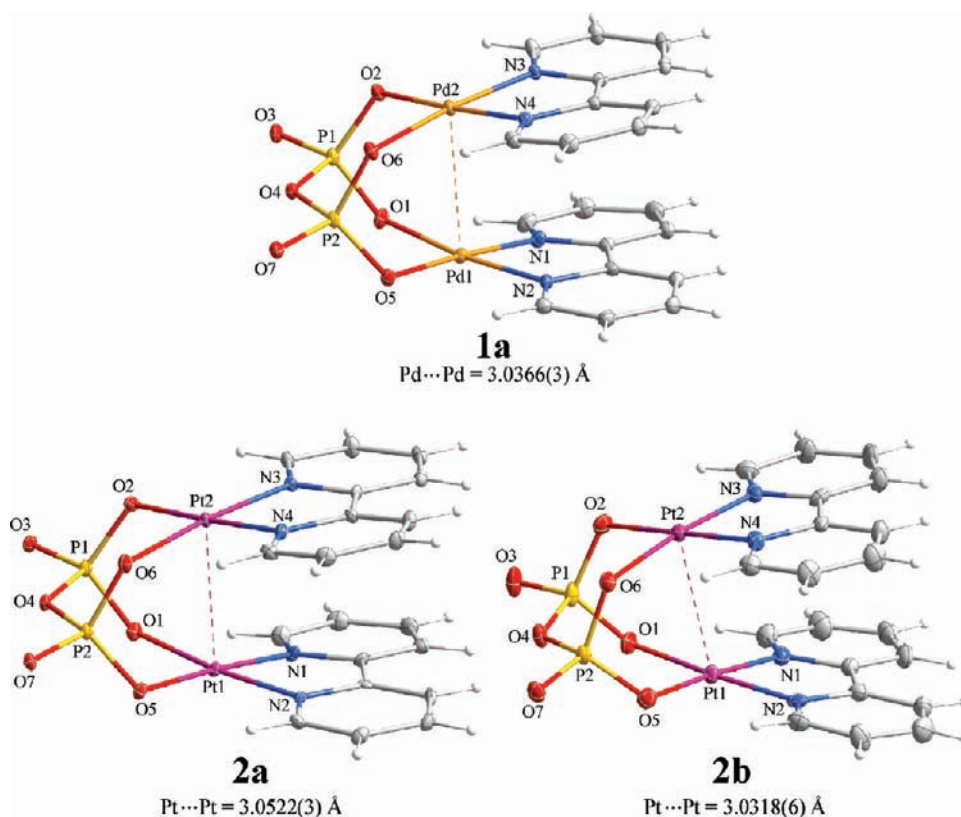
Figure 4. ORTEP (30% probability level) of the dimeric unit in **1**, **2a**, and **2b**, with the atom numbering scheme.

group, deep green polymorph). In each case, the crystallographic asymmetric unit is composed of the entire (noncentrosymmetric) dimeric unit and the solvent molecules. A perspective drawing of the $\{[M(bipy)]_2(\mu\text{-}P_2O_7)\}$ complex in **1a** and **2a/2b** is given in Figure 4; the same atom numbering scheme has been adopted for all compounds. Selected bond distances and angles are listed in Table 2, while details of bonds involving hydrogen atoms are given in Tables S1—S2 of the Supporting Information.

The structures of the two hexahydrated analogues **1a** and **2a** are virtually identical in terms of unit cell parameters (Table 1) and atomic positions, either within the dimeric unit or the solvent region. In both cases, the distance between the two metal centers is around 3 Å [3.0366(3) Å in **1a** (3.0511(3) Å according to ref 12) and 3.0522(3) Å in **2a**]. This is consistent with a weak d^8–d^8 interaction (the sum of the van der Waals radii for Pd and Pt are 3.26 and 3.50 Å, respectively[33]), although geometrical constraints of the ligands may in principle be crucial in determining the metal—metal separation, and a theoretical investigation of the bonding is thus required to establish that (vide infra). The two bipy molecules do not deviate substantially from planarity, and the dihedral angle between their main plane is about 3.7—3.8°. The interplanar distance (calculated by averaging the distance from each ring centroid to the main plane defined by the opposite molecule) is about 3.5 Å. These values are indicative of a strong intramolecular π–π interaction. The dihedral angle between the two metals coordination planes is also very small for this class of "clamshell"-like complexes, being $17.0(1)°$ in **1a** and $17.5(1)°$ in **2a** (note that the O···O distance in the bridging O—P—O moiety is about 2.5 Å versus the 2.2—2.3 Å span offered by the most commonly used bridged ligands). The M—O and M—N distances are as expected, and the average torsion angles

Scheme III. M1 and M2 Coordination Planes
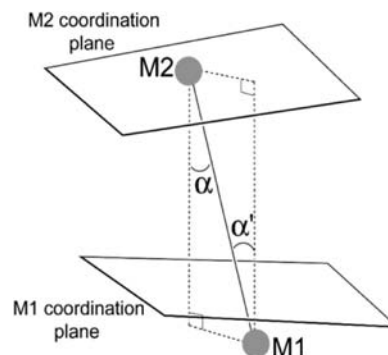
$[X—M1\cdots M2—X'; X = O, N]$ are about 5.1° in **1a** and 4.8° in **2a**.

The introduction of additional quantities here may be useful to provide a more detailed description of the molecular distortion along an "ideal" direction, normal to the average metal coordination plane (usually one of the unit cell axes): the dihedral angles between the M1—M2 direction and the direction of the projection (i) α, of M2 on the M1 mean plane, and (ii) α', of M1 on the M2 mean plane (Scheme III). For an ideal coplanar and eclipsed conformation, $\alpha = \alpha' = 0°$. For an eclipsed (but not coplanar) conformation $\alpha = \alpha' \neq 0°$, and for a noncoplanar and noneclipsed conformation, $\alpha \neq \alpha'$. In the case of **1a** and **2a**, α and α' assume values of 12.2 and 10.2°, and 11.9 and 10.3°, respectively. Beside accounting for the already noted small dihedral angle between the two metal ion coordination planes, these values also
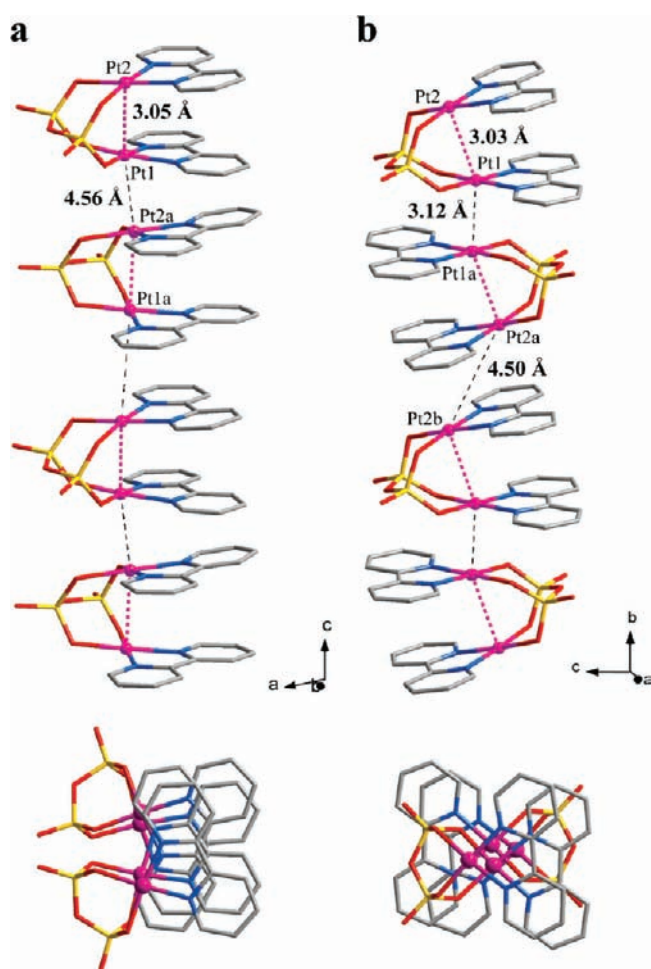
Figure 5. Side and top views of the 1-D arrangement of $[Pt(bipy)]_2(\mu\text{-}P_2O_7)]$ dimers in **2a** (a) [(a) $x, 1 - y, -0.5 + z$] and **2b** (b) [(a) $1.5 - x$, $0.5 - y, 1 - z$; (b) $+ x, 1 + y, + z$].

indicate that the two metal ions in the dimeric unit are almost perfectly eclipsed along an "ideal" axial direction, which in this case corresponds to the crystallographic c axis (Figure 5).

In the polymorph **2b**, the metal−metal separation is 3.0318(6) Å, while the interplanar distance between the two bipy molecules is about 3.5 Å, in agreement with that already observed in **2a** and **1a**. This suggests the nature of the bridging and capping ligands dictate key molecular parameters, independently from crystal packing effects. However, several slight differences can be noted between the dimeric molecule in **2a/1a** and **2b**. First, the dihedral angle between the two Pt^{II} ions coordination planes is 19.3(1)° in **2b**, and the angle between the two bipy main planes is 8.9(1)°, indicating a weaker intramolecular π−π overlap with respect to the one detected in the first two structures. The average torsion angle [X−M1$\cdots$M2−X'; X = O, N] is about 4.4°, while the previously defined α and α' angles assume values of 5.8° and 18.5°, respectively. This large difference between α and α', not noted in **2a/1a**, is an indication that in **2b** the two metal ion coordination planes are significantly shifted with respect to each other along the direction perpendicular to coordination (in this case, the crystallographic b axis), and in fact, the $\{[Pt(bipy)]_2(\mu\text{-}P_2O_7)\}$ unit is more "distorted" in **2b** with respect to **2a** (Figure 4).

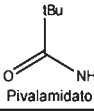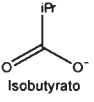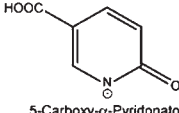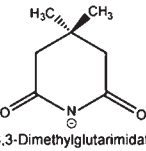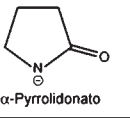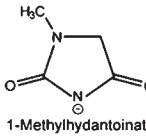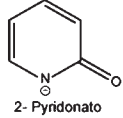The analysis of the crystal packing in **1a−2a/2b** revealed significant analogies and differences that can be found between the Cc and the $C2_1/c$ unit cells. In both cases, the dimeric units are arranged in supramolecular chains running along the crystallographic c (for **1a/2a**) or b (for **2b**) axis, mainly driven by hydrogen bonding interactions. Intermolecular π−π overlap between the bipy ligands are also observed in the Cc packing (**1a/2a**), with adjacent dimeric units twisted by about 60° with respect to one another (Figure 5a). This results in a zigzag arrangement of the dimeric units along the c axis, with long metal−metal intermolecular separations [4.5401(3) Å in **1a** and 4.5609(3) Å in **2a**] and M2−M1−M2a and M1−M2a−M1a angles of about 154 and 136° in **1a** and 155 and 137° in **2a**, respectively [(a) $x, 1 - y, -0.5 + z$, see Figure 5a]. No such interdimeric aromatic interactions are observed instead in the $C2_1/c$ unit cell, given that two closely packed dimeric units are related by an inversion center and, thus, tilted 180° with respect to one another (Figure 5b). The resultant *dimer-of-dimers* (*pseudo*-tetramer) structural submotif is characterized by interdimeric and intertetrameric Pt$\cdots$Pt distances of 3.1177(8) and 4.5033(9) Å, respectively, and Pt2−Pt1−Pt1a and Pt1a−Pt2a−Pt2b angles of about 151° and 137° [(a) $1.5 - x, 0.5 - y, 1 - z$; (b) $+ x, 1 + y, + z$, see Figure 5b].

The "clamshell"-like geometry adopted by this series of complexes, although not common, has been observed in a few other square planar Pd^{II} and Pt^{II} dimers characterized, as in **1** and **2**, by a mixed bridging/capping ligand set.[8,34i−34l] However, to the best of our knowledge, **1** and **2** represent two rare examples of isostructural[34] as well as neutral dinuclear Pd^{II} and Pt^{II} compounds. This latter point appears particularly relevant when considering the polymorphism exhibited by **2**. In fact, after a thorough search in the Cambridge Structural Database (November 2010), the occurrence of a similar packing variance could be only detected for one literature Pt^{II} species, the cationic complex of formula $\{[Pt(NH_3)_2]_2(\alpha\text{-pyrrolidonato})_2\}^{2+}$, which was found to crystallize as isolated dimers (P-1 space group, colorless crystals)[35] or "*dimer-of-dimers*" ($C2_1/c$ space group, brown-yellow crystals),[36e] depending on the presence of sulfate or mixed nitrate/hexafluorophosphate counterions, respectively. The existence of the two crystalline forms of **2**, given the neutral nature of the complex, is associated with solvation effects.

Interestingly, the "*dimer-of-dimers*" structural motif found in **2b** and the brown polymorph[36e] of the cited α-pyrrolidonato system, typical of the famous mixed-valent "platinum blue"[36] class of materials, is still quite unusual among Pt^{II} (Table 3)[36] or Pd^{II} complexes,[37] and it appears now well established that *pseudo*-tetranuclear structures of this type immediately separate into dimers upon dissolution in aqueous media.[36c] Of note, the pyrophosphato-dach [dach = *trans*-1,2-cyclohexanediamine] Pt^{II} analogue of formula $\{[Pt(dach)]_2(\mu\text{-}P_2O_7)\}\cdot 4H_2O\}$, recently described by Bose et al.,[7a] also shows this type of crystal packing, although no evidence of polymorphism have been reported by the authors for this species.

When analyzing the polymorphism exhibited by **2**, with interdimeric Pt$\cdots$Pt interactions present in the dark green ("black") polymorph **2b** but not in the orange phase **2a**, other structural considerations are due. For instance, an analogy between **2b−2a** and the crystal packing of the "red" ($Cmcm$ unit cell, close Pt$\cdots$Pt contacts) and "yellow" ($Pbca$ unit cell, long Pt$\cdots$Pt separations) forms of the prototypical Pt(bipy)Cl$_2$[32] monomer species can be easily found. Interestingly, although shorter intermolecular Pt$\cdots$Pt interactions have been found to generally result in less dense structures,[38] this principle does not apply to **2a** and **2b** (Table 1).

2514

dx.doi.org/10.1021/ic1023373 |*Inorg. Chem.* 2011, 50, 2507–2520

Table 3. Dimeric Pt^{II} Complexes with a *Dimer-of-Dimers* (*Pseudo*-Tetramer) Packing Motif^{a,b}

Bridging ligand	Co-ligand	Counterion	Crystallization solvent	Space group	M-M distance/Å ^{b}	Crystal color	CCDC Refcode (ref)
PPi	dach	-	H$_2$O	P-1	3.372 / *3.237*	colorless	(7a)
Pivalamidato (tBu)	dach, NH$_3$	ClO$_4^-$	acetone	P21/n	3.037 / *3.226*	colorless	GELYIG (36a)
Isobutyrato (iPr)	NH$_3$	ClO$_4^-$	-	P-1	2.988, 3.025 / *3.262, 3.305*	yellow	IQUGUW (36b)
5-Carboxy-α-Pyridonato	NH$_3$	NO$_3^-$	H$_2$O	C2/c	2.902 / *3.182*	dark green	AJUHOC (36c)
3,3-Dimethylglutarimidato	bipy	NO$_3^-$	H$_2$O	P-1	2.833, 2.845 / *3.201*	deep violet	WIMJUX (36d)
α-Pyrrolidonato	NH$_3$	PF$_6^-$, NO$_3^-$	H$_2$O	C2/c	3.029 / *3.185*	brown-yellow	JASMOF (36e)
1-Methylhydantoinato	NH$_3$	NO$_3^-$	H$_2$O	P-1	3.131 / *3.204*	yellow	BOTFIZ (36f)
2-Pyridonato	en	NO$_3^-$	-	P21/c	2.991 / *3.235*	yellow	CATMEP (36g)
2-Pyridonato	NH$_3$	NO$_3^-$	-	P21/n	2.877 / *3.129*	green-yellow	PRDPTC (36h)

^{a} CCDC search November 2010. ^{b} Intradimeric distance, *interdimers (intratetrameric) distance.*

Electrochemistry. Cyclic voltammograms of **1**−**2** in aqueous 0.1 M KNO$_3$ are shown in Figures 6 and 7. Note that CVs were recorded at different pHs for **1**. ^{31}P NMR spectroscopy was used to confirm that the KNO$_3$ electrolyte does not react with **1** or **2**, and it was demonstrated that the presence of KNO$_3$ does not interfere with the protonation event, which occurs around neutral pH. The CV of **1** at pH 10.5 shows two irreversible oxidations at 1.25 and 1.55 V versus NHE. By analogy to our previously described [(2-phenylpyridine)Pd(μ-X)]$_2$ and [(2-p-tolylpyridine)Pd(μ-X)]$_2$ (X = OAc$^-$, acetate; or TFAc$^-$, trifluoroacetate) systems,[8] we assign these to the Pd^{III}−Pd^{II}/Pd^{II}−Pd^{II} and the Pd^{III}−Pd^{III}/Pd^{II}−Pd^{III} couples. The potentials of the Pd^{II}−Pd^{III}/Pd^{II}−Pd^{II} as well as the Pd^{III}−Pd^{III}/Pd^{II}−Pd^{III} couples in **1** are also comparable with those reported recently for a binuclear palladium benzoquinoline acetate complex.[39] At pH 8.5, the CV of **1** still displays two irreversible oxidations, but the area under the peaks is diminished. At pH 5.5, no oxidations are observed. Presumably at pH 5.5, the solution only contains the protonated version of **1**, which would be expected to be much more difficult to oxidize. At pH 8.5, a

mixture of **1** and the protonated species is present, reducing the intensity of the observed oxidations. The CV of the Pt complex **2** is similar to the Pd complex. The voltammogram displays two *quasi*-reversible oxidations centered at 0.9 and 1.1 V versus NHE, and these have been assigned to the same oxidation events as for Pd. Not surprisingly, it is easier to oxidize the heavier transition metal. Preliminary attempts to produce Pd^{III} or Pt^{III} dimers by chemical oxidation of **1** or **2** failed, resulting instead in complex decomposition and formation of monomers with the metal ion in either a +2 or +4 oxidation state. In the case of platinum, a new species was isolated by reacting **2a** (or **2b**) with NaNO$_2$ and concentrated HNO$_3$, the Pt^{IV} monomer of formula Pt(bipy)(NO$_2$)$_2$Cl$_2$ (**3**, see Table 1 and the Supporting Information).

Photophysics. UV−vis absorption spectra of **1** and **2** are shown in Figure 8; molar absorptivity data are listed in Table 4. Both **1** and **2** obey Beer−Lambert's law in low concentration conditions (10^{-5}−10^{-6} M, see Experimental Section), which suggests that no aggregation of the dimeric units is occurring in solution.[8] The absorption profiles are similar for both Pt and Pd,
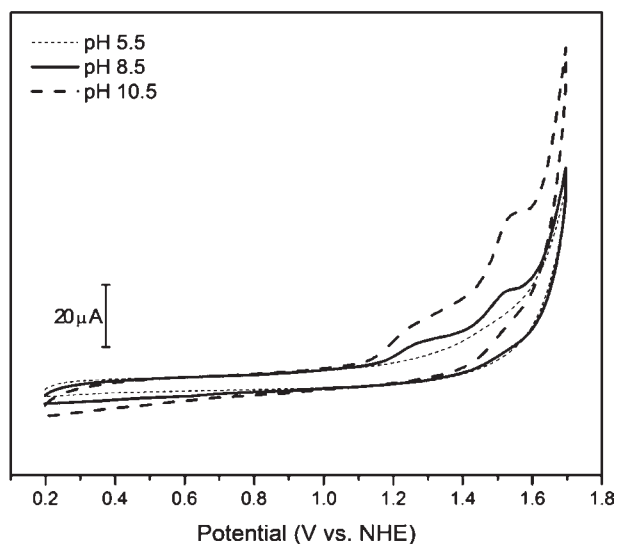
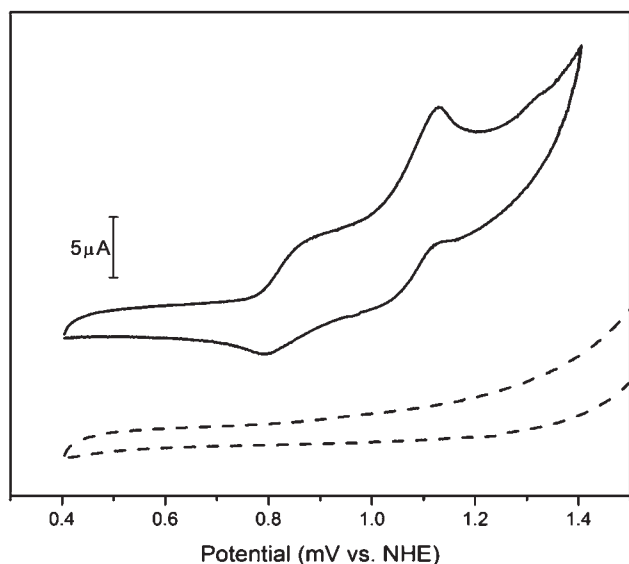**Figure 6.** Cyclic voltammogram of **1** in aqueous 0.1 M KNO$_3$, at various pHs.

Figure 7. Cyclic voltammogram of **2** in aqueous 0.1 M KNO$_3$ (the dotted line is the 0.1 M KNO$_3$ control).

and neither compound absorbs strongly in the visible region. The high energy peaks are probably attributable to [π–π^*] intra-ligand (IL) transitions, while the peaks at the edge of the visible region are most likely the result of metal to ligand charge transfer.[8,9g,h] In most cases, the bands for the Pt species are found at slightly lower energy compared to the analogous bands in the Pd species, and an additional broad band is seen at 363 nm for **2**. The origin of this band is unclear at this time. In contrast to other d^8–d^8 dimers, luminescence was not detected from either **1** or **2** at room temperature upon excitation of any of the UV–vis bands. This is consistent with the results of our analysis of bonding (vide infra).

Density Functional Theory Analysis of Bonding in Compounds 1–2. As mentioned earlier, compounds **1** and **2** represent a rare example of isostructural Pd and Pt compounds,
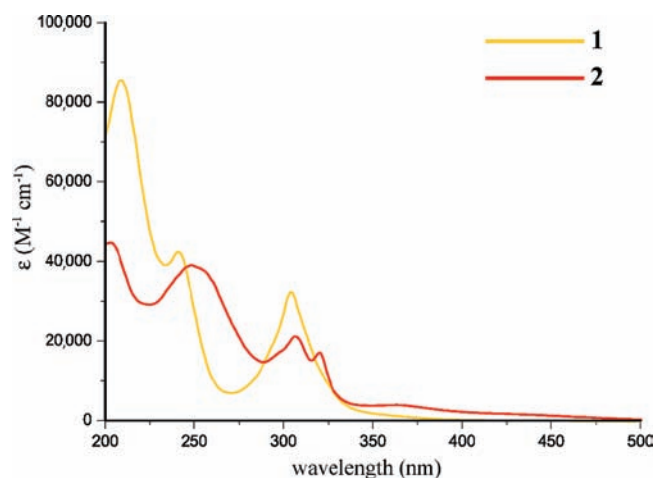

Figure 8. Electronic absorption spectra of **1** and **2** in water solutions (pH 7).

Table 4. Electronic Absorption Data for 1 and 2

	1		**2**
λ_{max} (nm)	ε_{max} (M^{-1} cm^{-1})	λ_{max} (nm)	ε_{max} (M^{-1} cm^{-1})
208.0	87200	203.0[a]	42700
241.0	41900	248.0	38500
304.0	32800	307.0	21000
		320.0	16800
		363.0	3850

[a] This band is observed at the edge of the spectral window, and the molar absorption coefficient may not be accurate.

which appear to potentially feature a d^8–d^8 interaction. We performed a DFT study in order to further understand the bonding in these species. In general, DFT is poor at modeling weak interactions such as π-stacking, hydrogen bonding, and van der Waals interactions.[40] Optimization of the geometry of **1** and **2** using density functional theory proved extremely difficult (Tables S6 and S7 of the Supporting Information). A variety of different functionals were tested, and the majority gave poor results. In general, functionals that gave the wrong structure predicted a "*pseudo*" planar geometry with no short metal··· metal distances and no intradimeric π–π stacking between the bipyridine rings. The exact reasons why some functionals performed better than other are unclear, and there appear to be no obvious trends for determining which functionals performed best. All pure functionals failed (TPSS could not even produce an optimized structure) and the performance of hybrid functionals was mixed. Interestingly, the hybrid functionals BH&H and BMK were able to reasonably accurately reproduce the experimental geometry for the Pd complex **1**, but failed for the Pt complex **2**. A MP2 calculation on **1** gave the correct "clamshell" geometry. However, the Pd···Pd distance was significantly shorter than the experimental value, and the molecule took almost one month to optimize on eight processors. The best results were obtained with the SVWN5 functional (see the Supporting Information for full comparison), which is essentially a local spin density approximation, and all further analysis was performed using this method.
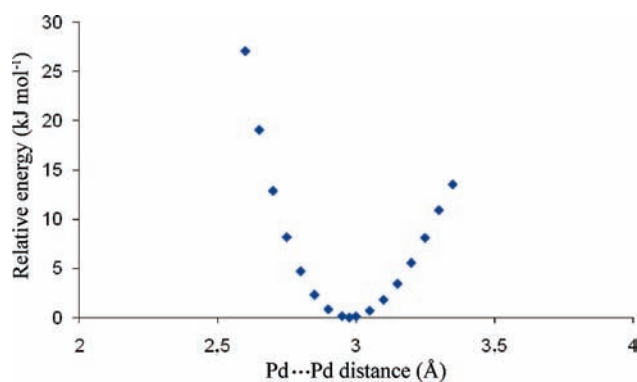
Figure 9. Graph of relative total energy of **1** as the intradimeric Pd···Pd distance is varied (the lowest energy point, Pd···Pd = 2.98 Å, is defined as 0).

In order to determine the importance of the M···M distance to the overall energy of the molecule, a linear transit calculation was performed on **1**. In this calculation, the Pd···Pd distance was held constant at several different values, while the rest of the molecule was optimized. The results are shown in Figure 9. Surprisingly, given the problems optimizing the structure of **1**, the potential well is reasonably steep, and small changes (anything greater than 0.15 Å) to the Pd···Pd distance result in a large change to the energy of the molecule. As the Pd···Pd distance is decreased, the bipyridine rings twist, so that the rings are no longer perfectly aligned. This geometry change presumably occurs because as the Pd···Pd distance is shortened, the rings are brought closer together, and the $\pi-\pi$ interactions start to become repulsive. In contrast, as the Pd···Pd distance is increased, the rings stay aligned, but the metal—metal interaction almost certainly becomes weaker. This suggests that the experimental metal—metal distance is a combination of the optimal distance for a metal—metal interaction and a $\pi-\pi$ interaction, although the importance of the geometrical constraint imposed by the PPi ligand is not easily derivable by this analysis.

In order to probe the bonding in **1** and **2**, a fragment analysis was performed in which the molecules were split into Pd_2 (or Pt_2), P_2O_7, and $(bipy)_2$ units. The calculations indicate that **1** and **2** possess the same electronic structure. In both cases the HOMO is a mixture of a d_{z^2} σ^* M—M antibonding orbital combined with the lone pairs of the oxygen atoms of the bridging pyrophosphate ligands, while the LUMO and close-lying empty orbitals are located on the bipyridine rings and possess mainly ligand character. The M—M σ-bonding character orbital (a mixture of both d_{z^2} and d_{xy}) is spread over three MOs and mixes with the pyrophosphate ligands. As expected, there are a number of occupied nonbonding metal orbitals and ligand-based orbitals between the HOMO and the M—M bonding orbitals. One of these orbitals, HOMO-5, includes another lower energy linear combination of the HOMO, a d_{z^2} σ^* M—M antibonding orbital combined with oxygen lone pairs. Selected molecular orbitals of **1** are shown in Figure 10. Table 5 gives the percentage contribution from the Pd^{II} or Pt^{II} ions to key orbitals of **1** and **2**, respectively.

The percentage contribution from the metal centers to the key orbitals involved in M—M bonding clearly demonstrates that mixing between the valence d_{z^2} and $(n+1)$ s and p orbitals is occurring. As expected from our previous studies, the contribution from the $(n+1)$ p and s orbitals is greater for Pt^{II} than Pd^{II}.[8] From the fragment analysis, a Pd—Pd bond order of 0.19 was
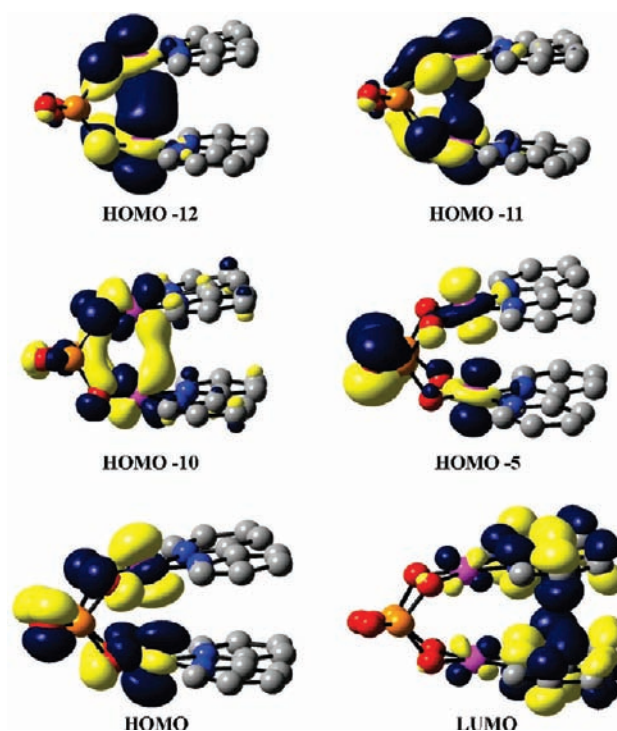

Figure 10. Selected molecular orbitals of **1**.

calculated for **1**, and a Pt—Pt bond order of 0.20 was calculated for **2**.[41] This is consistent with a weak bonding interaction. The AIM approach,[42] which uses topological analysis of the electron distribution to characterize bonding interactions, confirms the presence of metal—metal bonding interactions in **1** and **2**. In both cases, $(3, -1)$ bond critical points (indicative of the presence of a bonding interaction)[43] centered between the two Pd (or Pt) atoms were found. The ellipticity values were 0.06 for **1** and 0.04 for **2**, indicating a σ-bonding interaction.

From these calculations, it is clear that the bonding in **1** and **2** is very similar, and that both species feature a weak d^8-d^8 interaction. Because of the ligand-centered LUMO, upon excitation, the M—M bond order only increases by 0.5, and as a result **1** and **2** are not expected to display the photophysical properties of Pt, Rh, and Ir d^8-d^8 dimers, which undergo an increase in the M—M bond order of 1 upon excitation. The electronic structure of **1** is similar to those that we have previously described for a number of other d^8-d^8 Pd complexes; however, to the best of our knowledge, **2** is the first example of a Pt system with a clearly elucidated d^8-d^8 interaction, in which the bond order only increases by 0.5 upon excitation. It is likely that there are many other examples of Pt complexes of this type in which the bonding has not yet been examined.

On the basis of our results here and that of earlier reports,[8] we suggest that there should be two different classes for describing d^8-d^8 interactions in Pd^{II}, Pt^{II}, Rh^I, and Ir^I dimers. Class (i) encompasses species such as Pt-pop $\{Pt_2(\mu-P_2O_5H_2)_4^{4-}\}$[44] and $\{[Rh(CNPh)_4]_2^{2+}\}$[9a] in which there is an increase of approximately 1 in the M—M bond order upon excitation, whereas class (ii) comprises species such as $[(2\text{-phenylpyridine})Pd(\mu\text{-X})]_2$ (X = OAc^- or $TFAc^-$),[8] as well as complexes **1** and **2**, in which there is an increase of 0.5 in the M—M bond order upon excitation. Class (i) species are more likely to undergo photochemically initiated reactions, but in principle, it should be just as easy to

Table 5. Percentage Contribution from Pd or Pt to Key Orbitals of 1 and 2

orbital	Pd^{II} contribution in 1	Pt^{II} contribution in 2
HOMO-12	46% $4d_{z^2}$	33% $5d_{z^2}$
	4% 5s	19% 6s
	1% 5p	1% 5p
HOMO-11	28% $4d_{yz}$	20% $5d_{yz}$
	10% $4d_{z^2}$	3% $5d_{z^2}$
HOMO-10	43% d_{yz}	50% d_{xz}
HOMO-5	23% $4d_{z^2}$	4% $5d_{z^2}$
	6% 5s	3% 6s
HOMO	14% $4d_{z^2}$	20% 6s
	5% 5s	14% $5d_{z^2}$
	4% d_{xz}	8% d_{xz}
		2% 6p
LUMO	4% d_{xz}	5% d_{xz}

oxidize species from both categories, as this will cause the M—M bond order to increase to 1 in both cases. Computationally, it is straightforward to determine whether a species belongs in class (i) or class (ii) by looking at the nature of the LUMO; class (i) will have a LUMO that is weakly metal—metal bonding, whereas class (ii) will give a LUMO that is either ligand centered or metal—ligand antibonding in nature. Spectroscopy can also be used to differentiate between the two categories. To the best of our knowledge, all class (i) species give rise to fluorescence upon excitation of the M—M bond, whereas class (ii) species do not. In general, because of the unusually large energy gap between the Pd 4d_{z^2} and 5s/5p orbitals, Pd complexes are most likely to belong in class (ii), whereas Pt, Rh, and Ir species are more likely to belong in class (i). We have now shown that, with the right ancillary ligand, a Pt species that can be classified as class (ii) can be prepared.

■ CONCLUSIONS

Isostructural, "clamshell"-like, neutral dimeric PPi complexes of general formula $\{[M(bipy)]_2(\mu\text{-}P_2O_7)\}$ [M = Pd^{II} (1) or Pt^{II} (2)] have been synthesized and spectroscopically studied. Although the synthesis of the Pd^{II} species 1 is straightforward and high yielding, the synthesis of 2 is complicated and low yielding. Compound 2 can be synthesized starting from either Pt^{II} or Pt^{IV} precursors, and further work is required to understand the mechanism of PPi coordination and dimer formation. ^{31}P NMR studies indicate that both 1 and 2 undergo reversible protonation events at neutral pH, and higher synthetic yields may be obtained by carefully controlling the pH of the reaction mixture during complex synthesis. As part of this work, the solid-state structures of both 1 and 2 were elucidated. Two different polymorphs of 2 were obtained, and they reveal a strong dependence of the crystal color upon the presence/absence of Pt···Pt short contacts through the packing, which is in turn determined by a certain hydrogen bonding pattern (different in one polymorph to the other). One of the polymorphs of 2 is isostructural to the solid state structure of 1, and complexes 1 and 2 represent a rare example of isostructural neutral dinuclear Pd^{II}

and Pt^{II} compounds with a short M—M distances. The existence of two distinct crystalline phases of 2 is noteworthy because the phenomenon of polymorphism has been observed for the most part in mononuclear Pt^{II} species. DFT and AIM analyses showed that short M—M distance arises in part due to a weak d^8—d^8 interaction, and 1 and 2 have virtually identical electronic structures. In both cases, the HOMO is a weakly antibonding dσ* orbital, while the LUMO is a ligand-centered orbital, suggesting that on excitation the M—M bond order would only increase by 0.5. We have classified d^8—d^8 systems, which undergo an increase in M—M bond order of 0.5 upon excitation as class (ii) d^8—d^8 dimers. Class (i) d^8—d^8 dimers are those, which undergo an increase in M—M bond order of 1 on excitation. To the best of our knowledge, 2 is the first example of a Pt^{II} system that calculations have shown can be considered a class (ii) species. In contrast, at this stage it appears that all Pd^{II} d^8—d^8 dimers are class (ii), and it remains a challenge of the field to prepare Pd complexes that belong to class (i).

■ ASSOCIATED CONTENT

ⓈSupporting Information. Crystallographic data in CIF format for 1a, 2a, 2b, 3 and Pt(bipy)Cl$_4$; Figures S1—S2 on the 2b—2a transformation; additional NMR data (pH dependence in 0.1 KNO$_3$ solutions); mass spectroscopy (MALDI-TOF) data; hydrogen bonding interactions in 1a and 2a; ORTEP plot for 3; crystallographic details for Pt(bipy)Cl$_4$; and detailed DFT results. This material is available free of charge via the Internet at http://pubs.acs.org.

■ AUTHOR INFORMATION

Corresponding Author
*Phone: (1)-203-432-0885 (N.H.), (1)-315-443-4070 (R.P.D.). Fax: (1)-203-432-6144 (N.H.), (1)-315-443-4070 (R.P.D.). E-mail: nilay.hazari@yale.edu (N.H.), rpdoyle@syr.edu (R.P.D.)

■ ACKNOWLEDGMENT

■ REFERENCES

(1) *The Biochemistry of Inorganic Polyphosphates*, 2nd ed.; Kulaev, I. S., Vagabov, V., Kulakovskaya, T., Eds.; John Wiley & Sons: New York, 2004.

(2) (a) Walker, J. E. *Angew. Chem., Int. Ed.* 1998, 37, 2308. (b) Boyer, P. D. *Angew. Chem., Int. Ed.* 1998, 37, 2296.

(3) (a) *The Biochemistry of Nucleic Acids*, 10th ed.; Adams, R. L. P., Knowler, J. T., Leader, D. P., Eds.; Chapman and Hall: New York, 1986. (b) *Nucleic Acids in Chemistry and Biology*, 2nd ed.; Blackburn, G. M., Gait, M. J., Eds.; Oxford University Press: Oxford, 1996.

(4) Ikotun, O. F.; Marino, N.; Kruger, P. E.; Julve, M.; Doyle, R. P. *Coord. Chem. Rev.* 2010, 254, 890 and reference herein.

(5) (a) Marino, N; Vortherms, A. R.; Hoffman, A. E.; Doyle, R. P. *Inorg. Chem.* 2010, 49, 6790. (b) Ikotun, O. F.; Higbee, E. M.; Ouellette, W.; Doyle, R. P. *J. Inorg. Biochem.* 2009, 103, 1254. (c) Marino, N.; Mastropietro, T. F.; Armentano, D.; De Munno, G.; Doyle, R. P.; Lloret, F.; Julve, M. *Dalton Trans.* 2008, 38, 5152. (d) Ikotun, O. F.; Higbee, E. M.; Ouellette, W.; Lloret, F.; Julve, M.; Doyle, R. P. *Eur. J. Inorg. Chem.*

2008, 33, 528. (e) Ikotun, O. F.; Ouellette, W.; Lloret, F.; Kruger, P. E.; Julve, M.; Doyle, R. P. *Eur. J. Inorg. Chem.* **2008**, 17, 2691. (f) Ikotun, O. F.; Armatus, N. G.; Julve, M.; Kruger, P. E.; Lloret, F.; Nieuwenhuyzen, M.; Doyle, R. P. *Inorg. Chem.* **2007**, 46, 6668. (g) Doyle, R. P.; Nieuwenhuyzen, M.; Kruger, P. E. *Dalton Trans.* **2005**, 23, 3745. (h) Kruger, P. E.; Doyle, R. P.; Julve, M.; Lloret, F.; Niewenhuyzen, M. *Inorg. Chem.* **2001**, 40, 1726. (i) Marino, N.; Ikotun, O. F.; Julve, M.; Lloret, F.; Cano, J.; Doyle, R. P. *Inorg. Chem.* **2010**, in press.

(6) Xu, J.-Y.; Tian, J.-L.; Zhang, Q.-W.; Zhang, J.; Yan, S.-P.; Liao, D.-Z. *Inorg. Chem. Commun.* **2008**, 11, 69.

(7) (a) Mishur, R. J.; Zheng, C.; Gilbert, T. M.; Bose, R. N. *Inorg. Chem.* **2008**, 47, 7972. (b) Bose, R. N.; Maurmann, L.; Mishur, R. J.; Yasui, L.; Gupta, S.; Grayburn, W. S.; Hofstetter, H.; Salley, T. *Proc. Natl. Acad. Sci. (U.S.A.)* **2008**, 18314.

(8) Bercaw, J. E.; Durrell, A. C.; Gray, H. B.; Green, J. C.; Hazari, N.; Labinger, J. A.; Winkler, J. R. *Inorg. Chem.* **2010**, 49, 1801.

(9) (a) Mann, K. R.; Gordon, J. G.; Gray, H. B. *J. Am. Chem. Soc.* **1975**, 97, 3553. (b) Rice, S. F.; Milder, S. J.; Goldbeck, R. A.; Kliger, D. S.; Gray, H. B. *Coord. Chem. Rev.* **1982**, 43, 349. (c) Connick, W. B.; Marsh, R. E.; Schaefer, W. P.; Gray, H. B. *Inorg. Chem.* **1997**, 36, 913. (d) Osborn, R. S.; Rogers, D. *J. Chem. Soc., Dalton Trans.* **1974**, 1002. (e) Carr, N.; Crossley, J. G.; Dent, A. J.; Gouge, J. R.; Greaves, G. N.; Jarrett, P. S.; Orpen, A. G. *J. Chem. Soc., Chem. Commun.* **1990**, 11369. (f) Novoa, J. J.; Aullón, G.; Alemany, P.; Alvarez, S. *J. Am. Chem. Soc.* **1995**, 117, 7169. (g) Anbalagan, V. *J. Coord. Chem.* **2003**, 56, 161. (h) Maestri, M.; Sandrini, D.; Balzani, V.; Von Zelewsky, A.; Deuschel-Cornioley, C.; Jolliet, P. *Helv. Chim. Acta* **1988**, 71, 1053.

(10) Roundhill, D. M.; Gray, H. B.; Che, C.-M. *Acc. Chem. Res.* **1989**, 22, 55.

(11) (a) Clement, S.; Aly, S. M.; Bellows, D.; Fortin, D.; Strohmann, C.; Guyard, L.; Abd-El-Aziz, A. S.; Knorr, M.; Harvey, P. D. *Inorg. Chem.* **2009**, 9, 4118. (b) Pan, Q.-J.; Zhang, H.-X.; Zhou, X.; Fu, H.-G.; Yu, H.-T. *J. Phys. Chem. A* **2007**, 111, 287. (c) Xia, B.-H.; Che, C.-M.; Zhou, Z.-Y. *Chem.—Eur. J.* **2003**, 9, 3055. (d) Yip, H.-K.; Lai, T.-F.; Che, C.-M. *J. Chem. Soc., Dalton Trans.* **1991**, 1639. (e) Cotton, F. A.; Matusz, M.; Poli, R.; Feng, X. *J. Am. Chem. Soc.* **1988**, 110, 1144.

(12) While this contribution was in preparation, a short report on this structure appeared in Gao, J.; Riis-Johannessen, T; Scopelliti, R.; Qian, X; Severin, K. *Dalton Trans.* **2010**, 7114.

(13) Hambley, T. W. *Acta Crystallogr., Sect. C: Cryst. Struct. Commun* **1986**, 42, 49.

(14) *SMART, Data Collection Software*, version 4.050; Siemens Analytical Instruments, Inc.: Madison, WI, 1996.

(15) *SAINT, Data Reduction Software*, version 4.050; Siemens Analytical Instruments, Inc.: Madison, WI, 1996.

(16) Sheldrick, G. M. *SADABS*; University of Göttingen: Göttingen, Germany, 1996.

(17) Sheldrick, G. M. *SHELXTL PC*; Siemens Analytical X-Ray Instruments, Inc.: Madison, WI, 1993, and *SHELX97*; 1997.

(18) (a) *CrystalClear*; Rigaku Corporation: The Woodlands, TX, 1999. (b) *CrystalClear Software User's Guide*; Molecular Structure Corporation: The Woodlands, TX, 2000. (c) Pflugrath, J. W. *Acta Crystallogr.* **1999**, D55, 1718.

(19) *SIR2004: An Improved Tool for Crystal Structure Determination and Refinement*; Burla, M. C.; Caliandro, R.; Camalli, M.; Carrozzini, B.; Cascarano, G. L.; De Caro, L.; Giacovazzo, C.; Polidori, G.; Spagna, R., 2005.

(20) Cromer, D. T.; Waber, J. T. *International Tables for X-ray Crystallography*, Vol. IV; The Kynoch Press: Birmingham, England, 1974; Table 2.2 A.

(21) Ibers, J. A.; Hamilton, W. C. *Acta Crystallogr.* **1964**, 17, 781.

(22) Creagh, D. C.; McAuley, W. J. *International Tables for Crystallography*, Vol. C; Wilson, A.J.C., Ed.; Kluwer Academic Publishers: Boston, 1992; Table 4.2.6.8, pp 219−222.

(23) Creagh, D. C.; Hubbell, J. H. *International Tables for Crystallography*, Vol. C; Wilson, A.J.C., Ed.; Kluwer Academic Publishers: Boston, 1992; Table 4.2.4.3, pp 200−206.

(24) *CrystalStructure 4.0: Crystal Structure Analysis Package*; Rigaku and Rigaku Americas: The Woodlands, TX, 2000−2010.

(25) Gaussian 09, revision A.1; Frisch, M. J.; Trucks, G. W.; Schlegel, H. B.; Scuseria, G. E.; Robb, M. A.; Cheeseman, J. R.; Scalmani, G.; Barone, V.; Mennucci, B.; Petersson, G. A.; Nakatsuji, H.; Caricato, M.; Li, X.; Hratchian, H. P.; Izmaylov, A. F.; Bloino, J.; Zheng, G.; Sonnenberg, J. L.; Hada, M.; Ehara, M.; Toyota, K.; Fukuda, R.; Hasegawa, J.; Ishida, M.; Nakajima, T.; Honda, Y.; Kitao, O.; Nakai, H.; Vreven, T.; Montgomery, Jr., J. A.; Peralta, J. E.; Ogliaro, F.; Bearpark, M.; Heyd, J. J.; Brothers, E.; Kudin, K. N.; Staroverov, V. N.; Kobayashi, R.; Normand, J.; Raghavachari, K.; Rendell, A.; Burant, J. C.; Iyengar, S. S.; Tomasi, J.; Cossi, M.; Rega, N.; Millam, N. J.; Klene, M.; Knox, J. E.; Cross, J. B.; Bakken, V.; Adamo, C.; Jaramillo, J.; Gomperts, R.; Stratmann, R. E.; Yazyev, O.; Austin, A. J.; Cammi, R.; Pomelli, C.; Ochterski, J. W.; Martin, R. L.; Morokuma, K.; Zakrzewski, V. G.; Voth, G. A.; Salvador, P.; Dannenberg, J. J.; Dapprich, S.; Daniels, A. D.; Farkas, Ö.; Foresman, J. B.; Ortiz, J. V.; Cioslowski, J.; Fox, D. J. Gaussian, Inc.: Wallingford, CT, 2009.

(26) (a) Fonseca Guerra, C.; Snijder, J. G.; Te Velde, G.; Baerends, E. J. *Theor. Chem. Acc.* **1998**, 99, 391. (b) Te Velde, G.; Bickelhaupt, F. M.; Baerends, E. J.; Fonseca Guerra, C.; Van Gisbergen, S. J. A.; Snijders, J. G.; Ziegler, T. *J. Comput. Chem.* **2001**, 22, 931. (c) *ADF: Amsterdam Density Functional Software*; ADF2007.01; Science Computing & Modeling (SCM), Theoretical Chemistry, Vrije Universiteit: Amsterdam, The Netherlands, http://www.scm.com.

(27) (a) Vanlenthe, E.; Baerends, E. J.; Snijders, J. G. *J. Chem. Phys.* **1993**, 99, 4597. (b) Vanlenthe, E.; Baerends, E. J.; Snijders, J. G. *J. Chem. Phys.* **1994**, 101, 9783. (c) Vanlenthe, E.; Baerends, E. J.; Snijders, J. G. *J. Chem. Phys.* **1996**, 105, 6505. (d) Vanlenthe, E.; Ehlers, A.; Baerends, E. J. *J. Chem. Phys.* **1999**, 110, 8943. (e) Vanlenthe, E.; VanLeeuwen, R.; Baerends, E. J.; Snijders, J. G. *Int. J. Quantum Chem.* **1996**, 57, 281.

(28) Vosko, S. H.; Wilk, L.; Nusair, M. *Can. J. Phys.* **1980**, 58, 1200.

(29) Alba, J. C. O.; Jané, C. B. *XAim*; 1998. http://www.quimica.urv.es/XAIM/.

(30) *Infrared and Raman Spectra of Inorganic and Coordination Compounds, Part B, Applications in Coordination, Organometallics and Bioinorganic Chemistry*, 5th ed.; Nakamoto, K., Ed.; Wiley: Chichester, 1997.

(31) Pastoriza-Santos, I; Liz-Marzán, L. M. *Langmuir* **1999**, 15, 948.

(32) (a) Morgan, G. T.; Burstall, F. H. *J. Chem. Soc.* **1934**, 695. (b) Osborn, R. S.; Rogers, D. *J. Chem. Soc., Dalton Trans.* **1974**, 1002. (c) Textor, M.; Oswald, H. R. *Z. Anorg. Allg. Chem.* **1974**, 407, 244. (d) Canty, A. J.; Skelton, B. W.; Traill, P. R.; White, A. H. *Aust. J. Chem.* **1992**, 45, 417. (e) Connick, W. B.; Henling, L. M.; Marsh, R. E.; Gray, H. B. *Inorg. Chem.* **1996**, 35, 6261.

(33) Bondi, A. *J. Phys. Chem.* **1964**, 68, 441.

(34) Other examples of isostructural but charged Pd^{II} and Pt^{II} species can be found among (a) Kubiak, M. *Acta Crystallogr., Sect.C: Cryst. Struct.Commun.* **1985**, 41, 1288. (b) Vuoti, S.; Haukka, M.; Pursiainen, J. *Acta Crystallogr., Sect.C: Cryst. Struct. Commun.* **2007**, 63, m601. (c) En-Jun, G.; Ke-Hua, W.; Xiao-Fu, G.; Ying, Y.; Ya-Guang, S.; Wang-Zhong, Z.; Hong-Xi, Y.; Qiong, W.; Ming-Chang, Z.; Xiao-Mei, Y. *J. Inorg. Biochem.* **2007**, 101, 1404. (d) Raper, E. S.; Britton, A. M.; Creighton, J. R.; Clegg, W.; Hooper, M.; Kubiak, M. *Acta Crystallogr., Sect.C: Cryst. Struct. Commun.* **1987**, 43, 1538. (e) Cotton, F. A.; Matusz, M.; Poli, R.; Feng, X. *J. Am. Chem. Soc.* **1988**, 110, 1144. (f) Cotton, F.A.; Matonic, J. H.; Murillo, C. A. *Inorg. Chim. Acta* **1997**, 264, 61. (g) Cotton, F. A.; Matonic, J. H.; Murillo, C. A. *Inorg. Chem. Acta* **1996**, 35, 498. (h) Miguel, P. J. S.; Roitzsch, M.; Yin, L.; Lax, P. M.; Holland, L.; Krizanovic, O.; Lutterbeck, M.; Schurmann, M.; Fusch, E. C.; Lippert, B. *Dalton Trans.* **2009**, 10774. (i) Paschke, N.; Rondigs, A.; Poppenborg, H.; Wolff, J. E. A.; Krebs, B. *Inorg. Chim. Acta* **1997**, 264, 239. (j) Engelking, H.; Krebs, B. *J. Chem. Soc., Dalton Trans.* **1996**, 2409. (k) Borriello, C.; Centore, R.; Roviello, G. *Inorg. Chem. Commun.* **2005**, 8, 755. (l) Fedotova, T. N.; Aleksandrov, G. G.; Kuznetsova, G. N. *Zh. Neorg. Khim. (Russ.) (Russ. J. Inorg. Chem.)* **2008**, 53, 420.

(35) Sakai, K.; Sakai, I.; Draper, N. D.; Leznoff, D. B. *Acta Crystallogr., Sect. E: Struct. Rep. Online* **2004**, *60*, m273.

(36) (a) Fenghui Liu, W.; Chen, D. W. *Dalton Trans.* **2006**, 3445. (b) Sakai, K.; Ishigami, E. *Acta Crystallogr., Sect. E: Struct. Rep. Online* **2004**, *60*, m65. (c) Sakai, K.; Takahashi, S. *Acta Crystallogr., Sect. E: Struct. Rep. Online* **2003**, *59*, m532. (d) Matsumoto, K; Urata, H. *Chem. Lett.* **1993**, 2061. (e) Matsumoto, K.; Miyamae, H.; Moriyama, H. *Inorg. Chem.* **1989**, *28*, 2959. (f) Laurent, J.-P.; Lepage, P.; Dahan, F. *J. Am. Chem. Soc.* **1982**, *104*, 7335. (g) Hollis, L. S.; Lippard, S. J. *Inorg. Chem.* **1983**, *22*, 2600. (h) Hollis, L. S.; Lippard, S. J. *J. Am. Chem. Soc.* **1981**, *103*, 123.

(37) Examples of Pd[II] complexes showing a *dimer-of-dimers* solid state arrangement can be found in (a) Iwatsuki, S.; Itou, T.; Ito, H.; Mori, H.; Uemura, K.; Yokomori, Y.; Ishihara, K.; Matsumoto, K. *Dalton Trans.* **2006**, 1497. (b) Soro, B.; Stoccoro, S.; Minghetti, G.; Zucca, A.; Cinellu, M. A.; Gladiali, S.; Manassero, M.; Sansoni, M. *Organometallics* **2005**, *24*, 53. (c) Shu-Yan, Yu; Fujita, M.; Yamaguchi, K. *J. Chem. Soc., Dalton Trans.* **2001**, 3415. (d) Guang-Quan Mei, K.-L.; Huang, H.-P. *Acta Crystallogr., Sect. E: Struct. Rep. Online* **2007**, *63*, m2510. (e) Eremenko, I. L.; Nefedov, S. E.; Sidorov, A. A.; Ponina, M. O.; Danilov, P. V.; Stromnova, T. A.; Stolarov, I. P.; Katser, S. B.; Orlova, S. T.; Vargaftik, M. N.; Moiseev, I. I.; Ustynyuk, Yu A. *J. Organomet. Chem.* **1998**, *551*, 171. (f) Adrian, R. A.; Zhu, S.; Powell, D. R.; Broker, G. A.; Tiekink, E. R. T.; Walmsley, J. A. *Dalton Trans.* **2007**, 4399. (g) Mossi, W.; Klaus, A. J.; Rys, P.; Currao, A.; Nesper, R. *Acta Crystallogr., Sect. C: Cryst. Struct. Commun* **1995**, *51*, 2549.

(38) Grzesiak, A. L.; Matzger, A. J. *Inorg. Chem.* **2007**, *46*, 453 and references herein.

(39) Powers, D. C.; Ritter, T. *Nat. Chem.* **2009**, *1*, 302.

(40) Flener-Lovitt, C.; Woon, D. E.; Dunning, T. H.; Girolami, G. S. *J. Phys. Chem. A* **2010**, *114*, 1843.

(41) Cloke, F. G. N.; Green, J. C.; Jardine, C. N.; Kuchta, M. C. *Organometallics* **1999**, *18*, 1087.

(42) Bader, R. F. W. *Atoms in Molecules: A Quantum Theory*; Oxford University Press: New York, 1994.

(43) Bader, R. F. W. *Chem. Rev.* **1991**, *91*, 893.

(44) Roundhill, D. M.; Gray, H. B.; Che, C.-M. *Acc. Chem. Res.* **1989**, *22*, 55.